CrossMark

Global-mean surface temperature variability: space–time perspective from rotated EOFs

Xianyao Chen[1,2] · Ka-Kit Tung[3] (ID)

Abstract The observed global-mean surface temperature (GST) has been warming in the presence of increasing atmospheric concentration of greenhouse gases, but its rise has not been monotonic. Attention has increasingly been focused on the prominent variations about the linear trend in GST, especially on interdecadal and multidecadal time scales. When the sea-surface temperature (SST) and the land- plus-ocean surface temperature (ST) are averaged globally to yield the global-mean SST (GSST) and the GST, respectively, spatial information is lost. Information on both space and time is needed to properly identify the modes of variability on interannual, decadal, interdecadal and multidecadal time scales contributing to the GSST and GST variability. Empirical Orthogonal Function (EOF) analysis is usually employed to extract the space–time modes of climate variability. Here we use the method of pair-wise rotation of the principal components (PCs) to extract the modes in these time-scale bands and obtain global spatial EOFs that correspond closely with regionally defined climate modes. Global averaging these clearly identified global modes allows us to reconstruct GSST and GST, and in the process identify their components. The results are: Pacific contributes to the global mean variation mostly on the interannual time scale through El Nino-Southern Oscillation (ENSO) and its teleconnections, while the Atlantic contributes strongly to the global mean on the multidecadal time scale through the interhemispheric mode called the Atlantic Multidecadal Oscillation (AMO). The Pacific Decadal Oscillation (PDO) has twice as large a variance as the AMO, but its contribution to GST is only 1/10 that of the AMO because of its compensating patterns of cold and warm SST in northwest and northeast Pacific. Its teleconnection pattern, the Pacific/North America (PNA) pattern over land, is also found to be self-cancelling when globally averaged because of its alternating warm and cold centers. The Interdecadal Pacific Oscillation (IPO) is not a separate mode of variability but contains AMO and PDO. It contributes little to the global mean, and what it contributes is mainly through its AMO component. A better definition of a Pacific low-frequency variability is through the IPO Tripole Index (TPI), using difference of averaged SST in different regions of the Pacific. It also has no contribution to the GSST and GST due to the PDO being its main component.

1 Introduction

It has often been noted that the observed global-mean surface temperature (GST) has prominent variations about the positive trend of global warming. In addition to the response to time-varying anthropogenic and natural forcing, there are some major modes of internal variability arising from the oceans. The oceans are the source of low-frequency variability because of their higher heat capacity compared to the atmosphere and land. These forms of variability manifest themselves as sea-surface temperature (SST) quasi-oscillations usually identified from their distinct spatial

✉ Ka-Kit Tung
  ktung@uw.edu

[1] Physical Oceanography Laboratory/CIMST, Ocean University of China, Qingdao 266100, China

[2] Qingdao National Laboratory of Marine Science and Technology, Qingdao 266100, China

[3] Department of Applied Mathematics, University of Washington, Seattle, WA, USA

patterns and frequency bands. On interannual time scale, there are large variations of the tropical Pacific SST due to El Nino-Southern Oscillation (ENSO) (McPhaden et al. 2006; Sarachik and Cane 2010), with warm El Nino episodes and cold La Nina episodes affecting the global-mean land–ocean surface temperature with the same sign through teleconnections from the tropics to the extratropics (Wallace and Gutzler 1981; Simmons et al. 1983). On longer time scales, the attribution of the global-mean variation to various climate modes of variability is more controversial. There may exist two additional major modes of climate variability in the SST of the Pacific Ocean: the Pacific Decadal Oscillation (PDO) on decadal time scale (Mantua et al. 1997; Minobe 1999), and the Interdecadal Pacific Oscillation (IPO), which, as its name implies, is interdecadal and a pan-Pacific mode of variability (Folland et al. 1999; Power et al. 1999; Parker et al. 2007). In the Atlantic basin there is a prominent variability of its SST on multidecadal time scale, called the Atlantic Multidecadal Oscillation (AMO) (Folland et al. 1986; Schlesinger and Ramankutty 1994; Delworth and Mann 2000; Schlesinger et al. 2000; Knight et al. 2005; Wu et al. 2011). It was thought that the AMO is largely responsible for the global-mean surface temperature variation in the 60–70 year time scale (Wu et al. 2011), although recently it has been proposed that it is the IPO that is responsible for such a multidecadal variation in the global mean (Meehl et al. 2016). The PDO has also been proposed for this role (Trenberth 2015). There is also the controversy on whether such a variation in the global mean is caused by time-varying anthropogenic aerosol forcing (Booth et al. 2012; Zhang et al. 2013).

One previous approach for gaining some information on the composition of the GST variation is to decompose this time series into its various characteristic timescales. Using the method of Ensemble Empirical Mode Decomposition (EEMD) (Wu and Huang 2009), Wu et al. (2011) extracted the component responsible for the multidecadal variation of the GST. Two-dimensional surface temperature was then projected onto this time component to yield the spatial structure of the mode that is responsible for the multidecadal variation of the global mean. It was found that the center of action of this mode is in the Atlantic, with a spatial pattern that resembles the AMO.

Figure 1 is an updated version of the figure in Wu et al. (2011). In addition to showing the multidecadal frequency, we present all frequency components in the following manner. We divide the variability into three groups: the "high frequencies" include all periods below 10 years, and the "low frequencies" include all frequencies with periods above 10 years. The latter includes decadal, interdecadal and multidecadal. The third group is the secular trend, defined as the non-oscillatory part of the time series (Wu et al. 2007). Figure 1a shows the observed global average of the HadCRUT4.5 land + ocean surface temperature (Brohan et al. 2006; Morice et al. 2012) (in black) and its smoothed version (in blue). The smoothed version is the sum of the secular trend (brown) and the low-frequency part (red) of the GST. The variable global warming rates can be seen clearly in the smoothed data, including the global warming slowdown in the twenty-first century and a prior such period in the mid twentieth century, as well as periods in between when global warming accelerated, with the interannual fluctuations (green) superimposed upon the smoothed, multidecadally varying, platform. The high-frequency fluctuation is mostly associated with ENSO, as its associated spatial pattern is the cold-tongue pattern in the equatorial Pacific, seen in Fig. 1d below 1a. The spatial pattern associated with the low-frequency (period longer than decadal) part of that time series is shown in Fig. 1c. The same procedure was previously used by Wu et al. (2011) to find the spatial SST pattern of the multidecadal mode with an average period of 65 years, except that here we broaden the frequency range to include the decadal and interdecadal in addition to multidecadal variability. The low-frequency SST pattern is dominated by the interhemispheric dipole in the Atlantic basin, similar to the AMO, being warm in the North Atlantic but cool in the South Atlantic and vice versa. The variance in the eastern tropical Pacific is much weaker at 0.32, about 1/6 that of the North Atlantic at 1.95. Wu et al. (2011) showed that the 65-year mode's center of action is in the Atlantic, with only a weak extension in the Pacific; our result agrees with that and additionally shows that variability in all time scales longer than decadal, and not just the 65-year mode, has no center of action in the Pacific. This result concerns only the source that causes the variability in the global-mean surface temperature. It does not imply that the climate modes themselves do not have a center of action in the Pacific. In fact the PDO has twice the variance of the AMO (see later).

This result is controversial given the above reviewed publications on the role of PDO and IPO on the GST variations. In the rest of this paper, we will study the major modes of climate variability and how they affect the global mean. The approach is from the opposite direction as that used in Fig. 1: We start with the full space–time information of the two dimension plus time SST field, and decompose it into identifiable EOFs and their PCs using the method of pairwise rotated principal component analysis (Chen et al. 2017) (hereafter CWT). After the modes are identified based on the space–time information available, we then take the global average of the EOFs to yield the components of the global-mean SST (GSST). The additional spatial information before the global averaging allows us to understand why the influence from the Pacific on the GSST is mostly at the high frequencies, and why the Pacific's decadal and interdecadal variability do not contribute much to GSST. Land-plus-ocean surface temperature is then used to obtain the
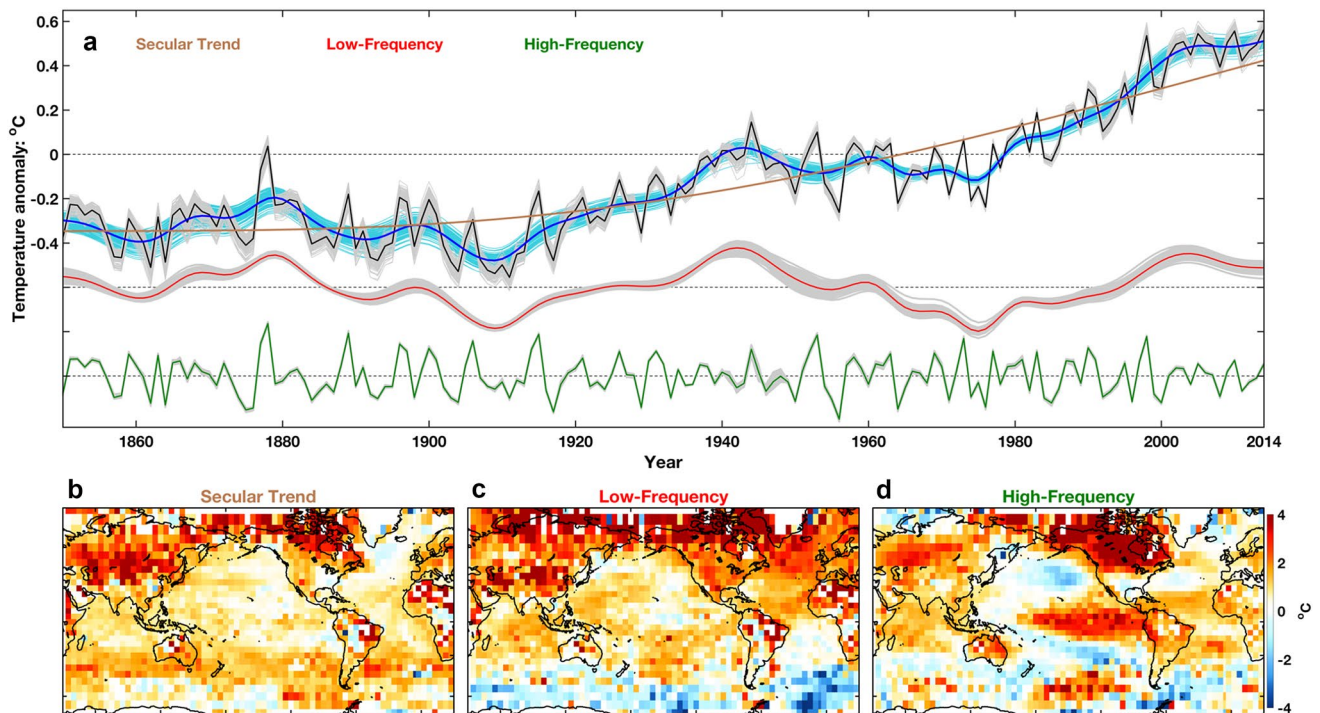
Fig. 1 Decomposition of the global mean temperature. One hundred ensemble members in the HadCRUT4.5 dataset, sampling systematic components of observational uncertainty, are shown in light grey. Their ensemble mean is in black. **a** Decomposition of each of the ensemble members of the HadCRUT4.5 global mean surface (land + ocean) temperature into its high-frequency (shorter than decadal; in green) and low-frequency (longer than decadal, in red) components. The secular trend is indicated with the brown line. The blue lines, consisting of the red and the brown lines, are seen as a good smoothed version of the original time series. The darker color line denotes the ensemble mean of the light color lines. The method used in the decomposition is ensemble empirical mode decomposition (Wu and Huang 2009) (EEMD), which has the advantage that it is lossless (the three components add up to the original time series perfectly) and that the high and low frequency components are constructed to be orthogonal (for all practical purposes in the implementation). The high-frequency component can also be seen as the difference between the original data and the smoothed version. Bottom panels: Spatial patterns obtained by regressing the global land + ocean surface temperature for the period 1910–2014 onto the secular trend (brown curve) (**b**); onto the low-frequency component (the red curve) (**c**); and the high-frequency component (the green curve) (**d**), after the low and high frequency time series are first normalized to unit standard deviation, so that the color shows the amplitude in degrees C. The left color scale is for the secular trend, while the right color scale is for the low and high frequency oscillations. The climatology is based on the 1961–1990 mean

spatial patterns of the corresponding modes of variability. These are then globally averaged to yield their contributions to the GST. This procedure helps us understand why the teleconnection patterns from the Pacific Ocean to land are not effective contributors to the global mean surface temperature at the low frequencies.

The use of rotated PCs in the decomposition of SST allows easier interpretation of the results. Our novel procedure of averaging the space–time decomposition from rotated EOF analysis is surprisingly simple. Because it has not been used previously to our knowledge as an orthogonal decomposition method for time series we provide here a simple mathematical derivation. It is applicable to any time series or indices based on global or regional SST. The application to GSST through area averaging is straightforward, and retains the orthogonality of the PCs. So the variance of each mode adds. The application to IPO involves low-pass filtering in time; the filtered PCs are no longer orthogonal. This creates mode mixing. Mode mixing provides the crucial information in answering the question: what is the IPO?

2 EOF decomposition of SST

The dataset used for constructing the oceans' climate modes is NOAA's ERSSTv.3b SST (Smith et al. 2008), with a 3-month running mean done in the preprocessing. Sensitivity of the rotated EOF analysis to a different dataset, namely HadISST, was discussed in CWT. Except for a weaker AMO amplitude in HadISST, most of the results remain similar in the two datasets.

The SST data is expressed in an orthogonal expansion of PCs in the form:

$$SST(\mathbf{x}, t) = \sum_{j=1}^{\infty} EOF_j(\mathbf{x})PC_j(t) \quad (1)$$

Both PCs and EOFs are orthogonal. The PCs are in addition normalized to have unit standard deviation.

We first show the conventional EOF decomposition of the SST in Fig. 2. This figure can be found in many previous publications, including CWT. It is included here for the purpose of contrasting with the rotated EOFs to be presented in Fig. 3. EOF1 is dominated by the global warming trend. Its time series, PC1, is almost indistinguishable from GSST (correlation coefficient r = 0.98). EOF2 contains ENSO in the tropical Pacific and is commonly referred to "ENSO-like" (Zhang et al. 1997). It has the shape of an equatorial cold tongue in the Pacific, and its PC is highly correlated (r = 0.86) with the ENSO index [the Cold Tongue Index

(CTI)] (Zhang et al. 1997). EOF3 has a spatial pattern with warming in the North Atlantic and cooling in the South Atlantic. Its PC time series is dominated by multidecadal scale variability and highly correlated with the AMO index (Enfield et al. 2001). The two time series are almost perfectly correlated at r = 0.98 if both are smoothed the same way. Without smoothing the PC, the correlation is still quite high (r = 0.82).

As pointed out by Chen and Wallace (2016), and seen in our Fig. 2., EOF2, the "ENSO-like" mode, is not a pure ENSO mode; it has the "bullet-like" feature of the PDO in the North Pacific mixed with the tropical ENSO pattern; the decadal variability of the PDO contributes to the mode mixing of PC2 in its frequency composition. The same North Pacific's feature is also found in EOF4. PC4's decadal frequencies are correlated with those of PC2, while its interannual frequencies are anti-correlated in such a way as to
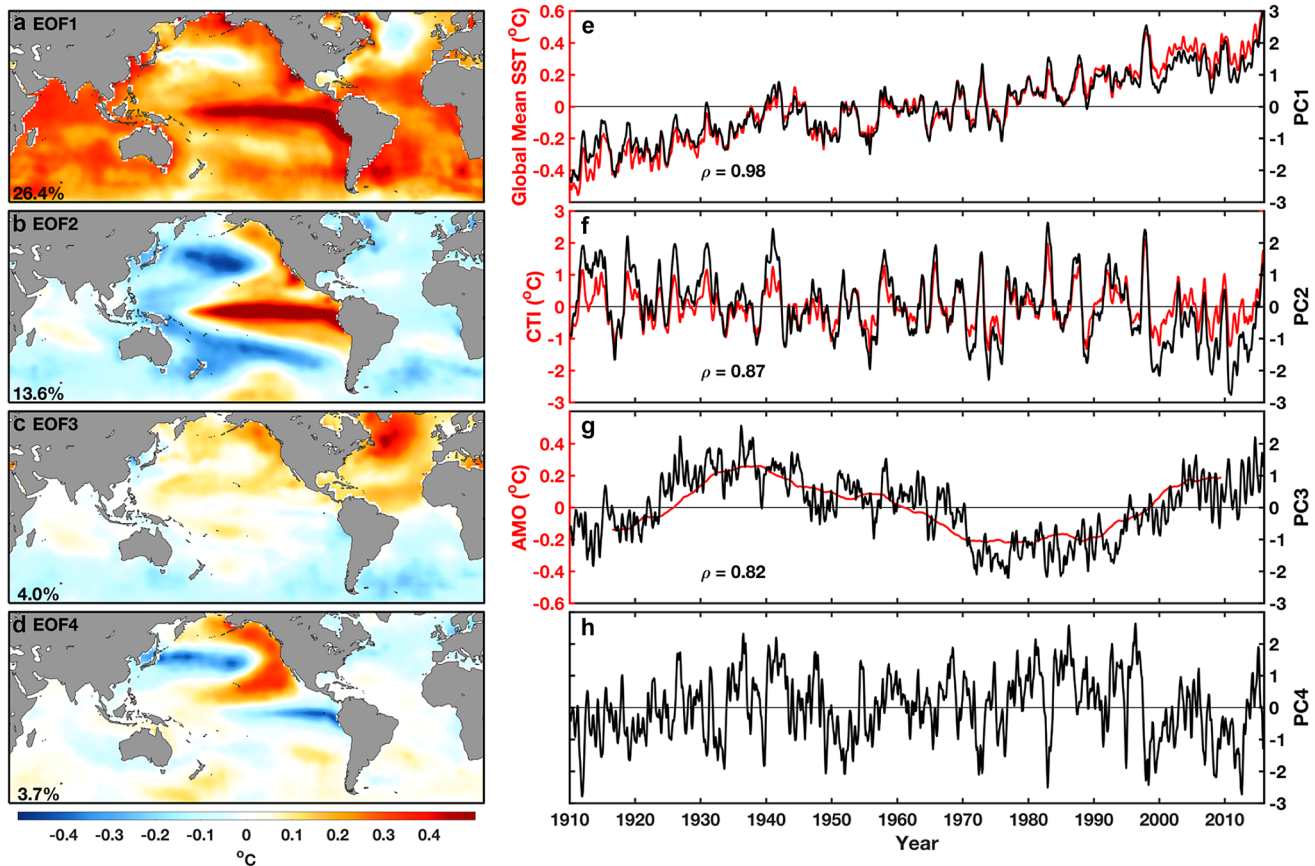
Fig. 2 Conventional EOF expansion of SST. (From top to bottom) The first four EOF modes (the left column) and their corresponding PC time series (black curves on the right column with the scale indicated on the right) obtained from three-month running mean SST of 1910–2015 with the seasonal cycle removed. The percentage of variance explained by each mode is displayed in the lower-left corner of each EOF panel. Over a thousand EOFs are used in calculating the percentage of variance. The PC time series from top to bottom are superimposed on the global mean SST anomaly, the cold tongue index (CTI) (Barnett 1984; Deser and Wallace 1987, 1990; Folland and Parker 1995; Zhang et al. 1997) and the AMO index of Enfield et al. (2001), respectively. The three indices are shown in red with the scale indicated on the left. The correlation coefficient between each PC and its corresponding index time series is indicated by ρ inside each panel. All the three ρ's are statistically significant at over 95% confidence level
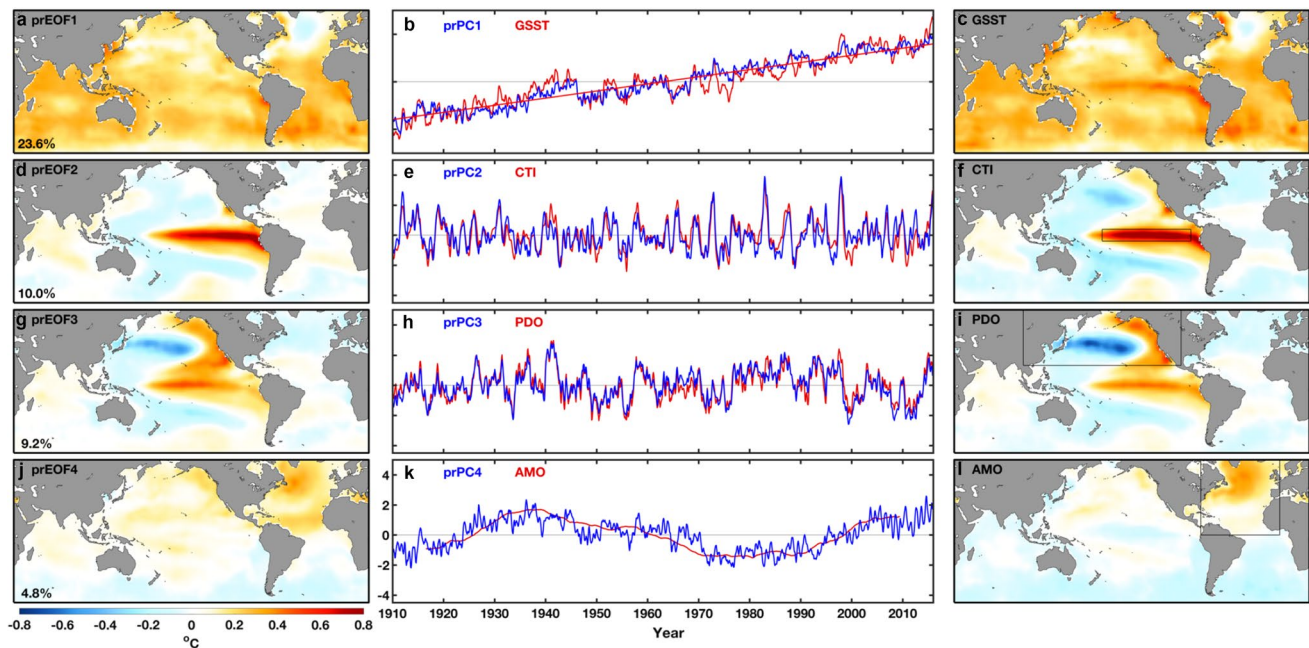
Fig. 3 Rotated SST EOFs and prPCs. Left column, the leading four rotated EOFs. Middle column: the rotated PCs in blue, and indices in red. Right column: the regionally defined indices and their global spatial patterns obtained through regression upon those indices. The regions used to define these indices are boxed

yield a zero overall correlation between PC2 and PC4, as required by the orthogonality constraint of the EOF analysis. These frequency bands can be largely decoupled if we simply add and subtract the two PCs (and divide by the square root of 2 to maintain the same normalization of unit standard deviation), as was done previously by Chen and Wallace (2016) for the case of pan-Pacific SST. The addition and subtraction are equivalent to 45- degree rotation of the pair of PCs. A detailed justification for the choice of the general rotation angle between a pair of PCs can be found in CWT, based on the minimization of mode mixing in the frequency bands between the pair. The optimal angle turns out to be 43 degrees. The spatial patterns from 43- and 45-degree rotations are visually indistinguishable. The pairwise rotated PCs (prPCs) are orthogonal and normalized, but the rotated EOFs are not necessarily orthogonal, which is an advantage because the physical modes themselves may not be spatially orthogonal. prPC1 contains all the linear trends: the other PCs' trends have been transferred to it, following the convention of CWT and Huang et al. (1998) that the dynamical modes are oscillations with zero trend. The trend transfer formula can be found in CWT.

The result is shown in Fig. 3. The rotated EOF2 is now the canonical ENSO, or variously called the Eastern Pacific ENSO or the ENSO-cycle mode. It has a large variance in the eastern coast of the Pacific Ocean and is more focused in the equatorial Pacific, and is "devoid of extratropical structure" (CWT). It is here referred to simply as the ENSO

mode. Its PC is dominated by the 2–7 year interannual frequencies, and highly correlated with the Cold-Tongue Index defined in Deser and Wallace (1987) (r = 0.83). Its global EOF spatial pattern is almost the same as the spatial pattern obtained by regressing global SST field onto this cold tongue regional mean index, shown in Fig. 3f, although the latter has slightly more structure in the North Pacific. prPC3 is virtually identical to the time series of the regionally defined PDO of Mantua et al. (1997) based on the leading PC of the SST north of 20N in the Pacific (r = 0.97 in 5-month running mean data). Its global EOF spatial pattern is close to the PDO's spatial regression pattern in Fig. 3i, except that the variability of our rotated global EOF3 along the equator is stronger in the central Pacific and tapers off to the eastern Pacific compared to the regressed one. The fourth mode closely resembles the Enfield et al. (2001)'s version of the AMO, which is defined as the ten-year running mean of linearly detrended Atlantic SST north of the equator.

Although the leading modes of variability obtained through our rotated PC analysis resemble the spatial patterns obtained by regressing global SST field onto the regionally defined climate indices, as shown in the middle and right columns of Fig. 3, the latter procedure cannot be used to reconstruct the SST field: first, these ad hoc indices are not necessarily orthogonal, and linear regression onto non-orthogonal indices may be problematic. Secondly the regressed spatial patterns are not ordered according to the global variance explained, and so we do not know if these

are the leading modes or if there are other missing modes in between them. Mathematically, the EOFs and their PCs can be used to reconstruct the SST field in the form of Eq. (1). The rotation of the PCs does not change the representation of the SST field expressed in Eq. (1) (as long as the PCs are still orthogonal), but gives it a better physical interpretation as its rotated PCs have largely distinct frequency ranges, and the EOFs, though global, have the familiar spatial patterns from previous regional definitions. We shall call the first EOF the global warming TREND (TR) mode, the second the ENSO mode, the third the PDO and the fourth the AMO.

Current understanding of the physical origin of the PDO was reviewed by Newman et al. (2016). In a paper entitled "ENSO-forced variability of the Pacific decadal oscillation", Newman et al. (2003) showed that variability on both interannual and decadal time scales of the PDO can be reproduced when tropical ENSO was introduced as a forcing term in an AR1 model. The "forecast" of the PDO using the simple model has considerably more skill than a simple AR1 model with only white noise forcing. The noise forcing represents noisy atmosphere-SST interactions in the extratropics. The AR1 mechanism is meant to incorporate the "reemergence" of North Pacific SST in subsequent winters of previous winter's ENSO forcing.

Newman et al. (2003)'s model is actually linear:

$$PDO(n) = a \cdot PDO(n-1) + b \cdot F(n) + w(n),$$

where the last term is white-noise forcing. We use the same model parameters, a and b as in Newman et al. (2003. The "ENSO" forcing (denoted by F here) that was used in Newman et al. (2003) is the leading PC of the tropical SST in a conventional EOF expansion. Its PC is similar to our ENSO-like mode in Fig. 2f. We can reexpress its PC into the pan Pacific modes. It is found to be:

$$F = F_1 + F_2, \quad \text{with} \quad F_1 = 0.8 \cdot ENSO, \quad \text{and } F_2 = 0.6 \cdot PDO.$$

In Fig. 4, we repeat the calculation of Newman et al. (2003) but in addition show the response of the model to each of the forcing components separately, and the sum of the two. The spatial pattern of the response is strikingly close to the forcing. This shows that the reason the extratropical PDO can be obtained through this AR1 model when only the "tropical ENSO" needs to prescribed as forcing is because there is a PDO contained in the forcing used in the form of F_2. When it is absent, and the forcing contains only ENSO, there is no extratropical PDO produced by this model. So the independence of ENSO and PDO modes, as we defined them through rotated EOFs, is likely more than a mathematical orthogonality result.

The relationship between AMO and PDO has been discussed in CWT. The AMO mode obtained from global SST has a center of action in the North Atlantic and a very weak extension in the North Pacific. On the other hand, PDO has no extension into the Atlantic. These two modes
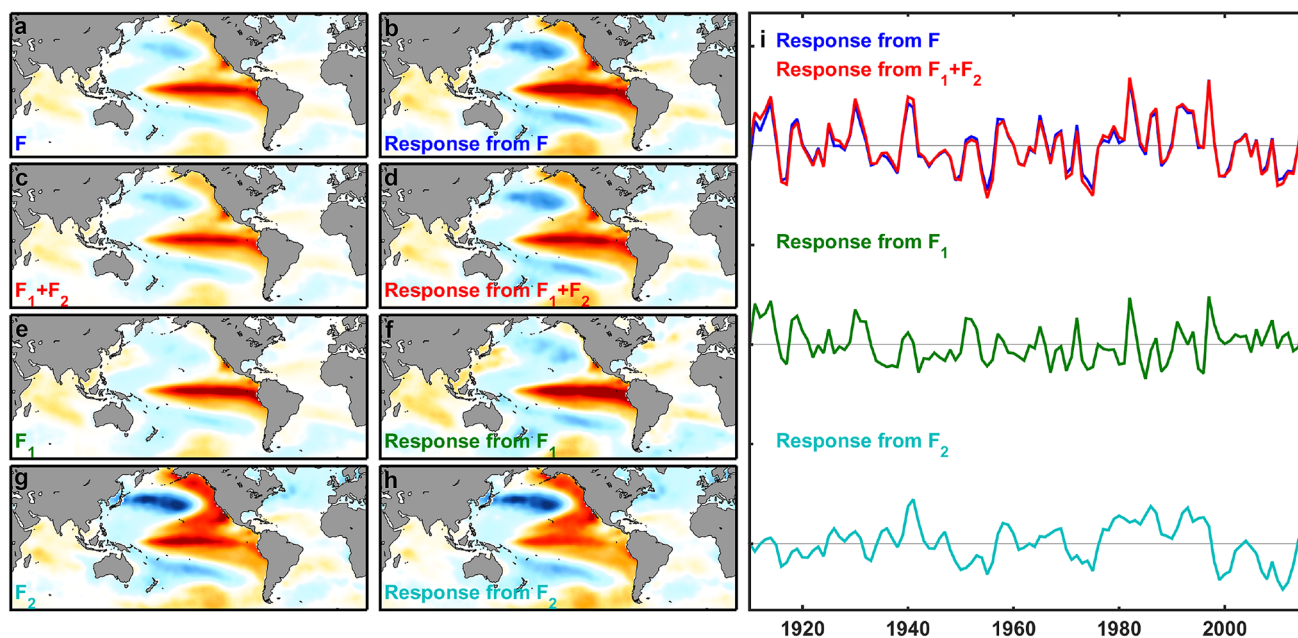
Fig. 4 Response of Newman's model to the two components of forcing used. Left column: the spatial pattern of the forcing used for Newman et al's (2003) model. (From top to bottom) The "ENSO" forcing that was the leading EOF/PC of tropical Pacific SST used in Newman et al. (2003), the forcing F = F₁ + F₂, the forcing F₁, and the forcing F₂. Middle column: the spatial pattern of different responses to the forcing in the left column based on Newman's model. Right column: the responses to the forcing F (blue), F₁ (green), and F₂ (cyan), and the summation of the responses to F₁ and F₂ (red), respectively

are mathematically uncorrelated. To investigate the physical connection between the two modes, CWT performed separate EOF analysis of the Atlantic basin and of the Pacific basin and found that the Atlantic pattern leads the weak Pacific signature by 15–20 years. The regression map of the global SST onto the mode in the Pacific basin has no notable signature in the Atlantic.

3 Components of global-mean SST

Equation (1) is rewritten as:

$$SST(\mathbf{x}, t) = TR(\mathbf{x}) \cdot prPC_1(t) + ENSO(\mathbf{x}) \cdot prPC_2(t)$$
$$+ PDO(\mathbf{x}) \cdot prPC_3(t) + AMO(\mathbf{x}) \cdot prPC_4(t) + \cdots \tag{2}$$

We take the global average, denoted by an overhead bar, of both sides of Eq. (2):

$$\overline{SST} = \overline{TR} \cdot prPC_1(t) + \overline{ENSO} \cdot prPC_2(t) + \overline{PDO} \cdot prPC_3(t)$$
$$+ \overline{AMO} \cdot prPC_4(t) + \cdots \tag{3}$$

Figure 4 shows the first four components of the global mean SST as given by Eq. (3); these four components comprise almost the entire GSST, as the remaining terms in the sum is negligibly small. (The right-hand side of Eq. (3) consists of orthogonal time series and so their variances add.) The first mode is the trend mode, due likely to global warming, but contains also artifacts of SST measurement after the end of the World War II (Thompson et al. 2009) and short term global cooling after major volcanic eruptions. The trend is about 0.08 °C per decade and is consistent with what was previously found using multiple regressions (Zhou and Tung 2013). It is seen that ENSO contributes to the global mean on the interannual scale and PDO mostly on the decadal scales, while the AMO has a clear multidecadal contribution. The AMO contributes about 0.25 °C to the global-mean SST (with a "trend" also of approximately 0.08 °C per decade) from trough to peak, which explains why when AMO was in its negative phase the observed global warming rate was noticeably smaller. ENSO's contribution to the global mean is only in the interannual range. PDO's contribution to the global mean is surprisingly small, considering that Pacific has a larger surface area than the Atlantic and the PDO has twice as much variance as the AMO before global averaging. The reason for its smaller global average is the PDO's spatial pattern, with its compensating warm and cold regions.

If conventional EOFs are used, the first PC is almost the same as GSST (see Fig. 2), already containing contributions of the dynamical modes to the GSST. Consequently, no information on its composition can be revealed since a PC cannot be further decomposed, except with the use of EMD, and this has been done and shown in Fig. 1.

4 Components of GST

Figure 5 shows that PDO has a much smaller direct contribution to the global mean SST variation compared to the AMO. However, it is known that tropical and Northern Pacific can generate teleconnections to the extratropics and over land. In particular, PDO has a close association with the atmospheric Pacific/North American (PNA) pattern, which exerts a strong influence on the surface air temperature (SAT) over North America. So it is possible that the indirect effect of the PDO on the global-mean land-plus-ocean surface temperature (GST) is not small. On the other hand, the PNA patterns have alternating warm and cold centers, and they may not be effective in forcing the global mean. We investigate this effect in Fig. 6 using HadCRUT4.5 land-plus-ocean surface temperature data.

Figure 6 shows the spatial structure obtained by regressing the land + ocean surface temperature onto each of the prPCs: TR, ENSO, PDO and AMO. The PDO mode does have a significant influence on the surface temperature of the North America continent. However, the eastern half of the content has a different polarity as the western half. This compensating warm-cold structure greatly reduces the global impact of the PDO mode. AMO, on the other hand, has teleconnections of the same sign over North America. Since the PCs have unit variance, the variance of the modes can be obtained from the EOFs alone. Taking the global mean of the spatial patterns yields, for each of the modes: TR (0.27), ENSO (0.04), PDO (0.01) and AMO (0.10), in degrees C. Thus the contribution to GST by PDO is only 1/10 that by AMO.

No lag is used in calculating the spatial patterns associated with the PDO-PNA teleconnections, and this is probably not needed, because the mechanism of the PNA teleconnection, by Rossby wave propagation (Horel and Wallace 1981; Hosking and Karoly 1981), should take less than a season. Since we use seasonal mean data, our result should include effects of this slight lag.

The components of GST are shown in Fig. 7. They are calculated using a formula similar to Eq. (3), but replacing SST by the land + ocean surface temperature, and using the global mean of the spatial patterns given above. Notice that the sum of the first four modes is a close approximation of the GST, meaning that the leading PCs calculated previously from EOF analysis of the SST field are also the leading ones for the land-plus-ocean surface temperature field. The slight differences occur during periods of bad (such as after WWII) and sparse (before 1930) data. The closeness of the GST

Fig. 5 The global mean SST.
Shown are the four orthogonal
components of the global-
mean SST of unfiltered data
as a function of time. Each
curve has been offset vertically
by 0.2. From top to bottom,
GSST and the sum of the
first 4 components, showing
that the latter is a very good
approximation of the former,
$\overline{TR} \cdot prPC_1(t), \overline{ENSO} \cdot prPC_2(t),$
$\overline{PDO} \cdot prPC_3(t)$ and $\overline{AMO} \cdot prPC_4(t)$
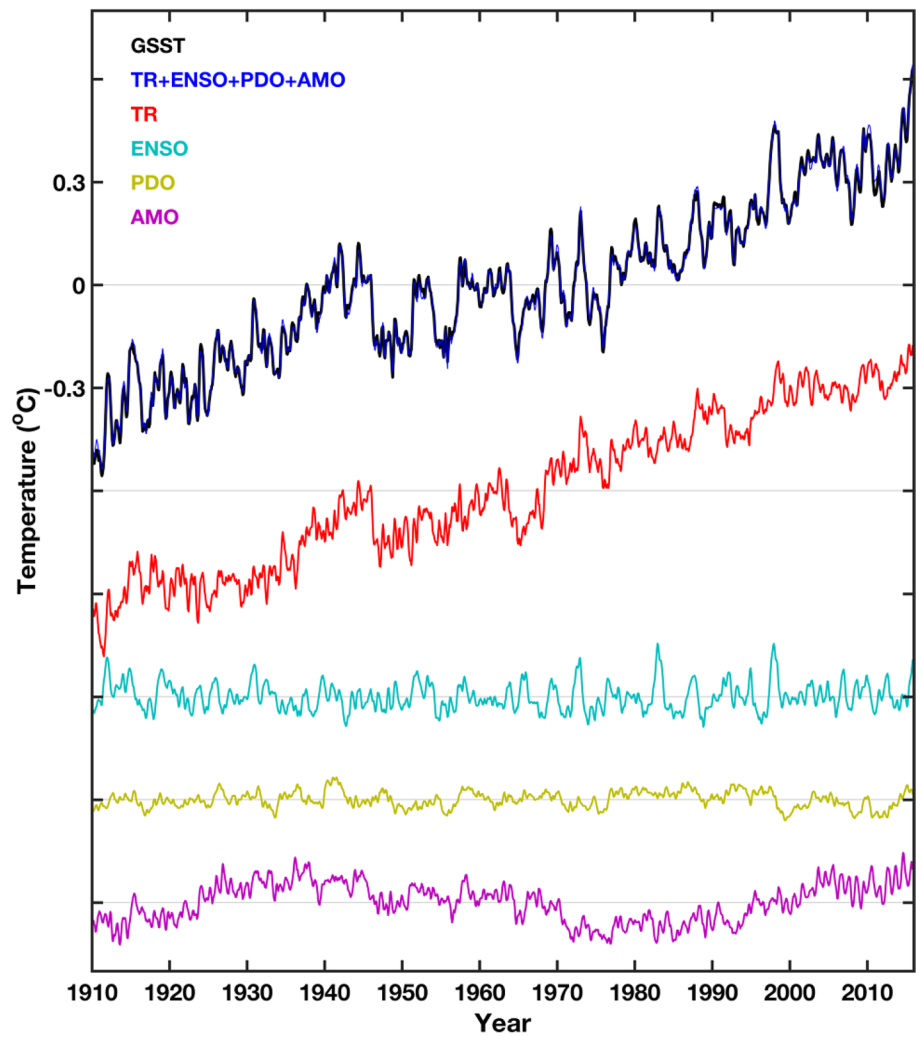
and the sum of the first four modes obtained without using
any lags shows that the lags are probably not significant in
influencing GST. The Atlantic is the main contribution to
the multidecadal variation of the GST through AMO. The
Pacific contributes only at interannual time scales through
ENSO.

5 The IPO

In an orthogonal EOF expansion of the SST, IPO does not
appear as one of the EOFs. Therefore the discussion of the
variations of SST in the previous sections is complete without
delving into the issue of what the IPO is. Nevertheless, due to
the frequent attributions of the variations of the GSST/GST to
an interdecadal variability referred to as the IPO, it would be
useful to reconcile the above-obtained results by calculating
the contribution to the global mean by the IPO.

The IPO is defined as the second EOF (after the global
warming mode) of decadally low-pass filtered SST according
to Parker et al. (2007) and Henley et al. (2015). This appears
to be the currently adopted definition, although IPO originally
was defined by Folland et al. (1999) and Power et al. (1999) as
the third EOF of 13.3-year low-pass SST.

The IPO is not a distinct climate mode, but a combina-
tion of the modes discussed above. The mixing of the existing
modes is caused by the low-pass filtering, since the filtered
PCs are not orthogonal. We apply a N-year Lanczos low-pass
filter, denoted by […] to both sides of Eq. (1) or (2). The deri-
vation below is the same whether the PCs are rotated or not:

$$[SST] = \sum_{j=1}^{\infty} EOF_j(\mathbf{x})\left[PC_j(t)\right]. \tag{4}$$

The filtered PCs are no longer orthogonal. Since filtering
also reduces their variances, they are also no longer normal-
ized. For presentation purpose, we renormalize the filtered
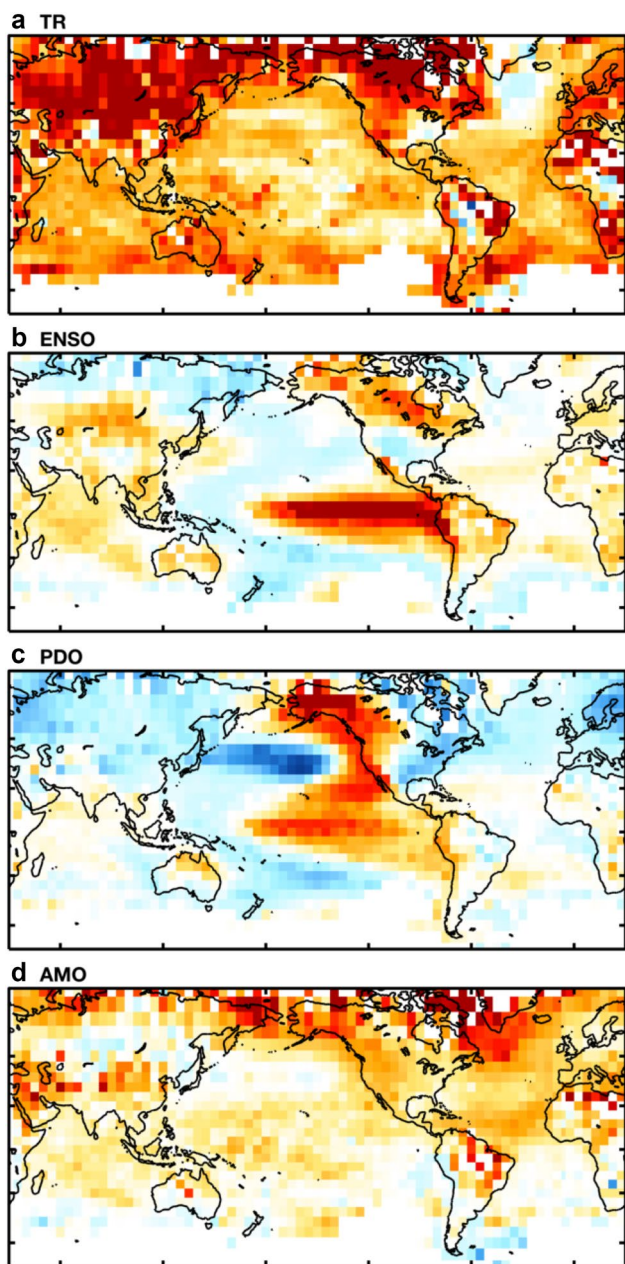
Fig. 6 Spatial land + ocean surface temperature patterns associated the four leading climate modes of variability: TR (**a**), ENSO (**b**), PDO (**c**) and AMO (**d**). Gridpoints where at least 1/3 of the data length for the period 1910–2015 are missing are left blank

PCs by their respective standard deviation, and the normalization constant is absorbed into the EOFs.

The low-pass filtered data on the left-hand side is expanded in a different orthogonal EOF expansion. We denote its (conventional) EOF by E and its PC by P. Both E and P are orthogonal. P is in addition normalized to unit standard deviation:

$$[SST(\mathbf{x},t)] = \sum_{i=1}^{\infty} E_i(\mathbf{x})P_i(t). \tag{5}$$

The IPO may either appear as P_2, or P_3.

The PCs of the filtered SST can be obtained by taking the spatial inner product $<.>$ of E_m on both sides of Eqs. (4) and (5), recalling that the E's are orthogonal, as:

$$P_m(t) = \sum_{j=1}^{\infty} \alpha_j \big[PC_j(t)\big] \tag{6}$$

$$\alpha_j = \frac{< EOF_j(\mathbf{x}) \cdot E_m(\mathbf{x}) >}{< E_m(\mathbf{x}) \cdot E_m(\mathbf{x}) >}.$$

We can also obtain the component of the EOFs of filtered SST. Taking the inner product of P_m on both sides of Eqs. (4) and (5), and recalling that the P's are orthogonal and has unit variance, we find:

$$E_m = \sum_{j=1}^{\infty} EOF_j \cdot < \big[PC_j\big] \cdot P_m >. \tag{7}$$

Globally averaging both sides of Eq. (7) then yields the global-mean components of the IPO for either m = 2 or 3.

Figure 8a shows the spatial patterns of the second EOFs of the 13-year low-pass filtered SST. The largest variance is in the North Atlantic, in a form similar to the AMO. Its PC, shown in Fig. 8c, is mainly multidecadal. On the other hand the spatial pattern for lower thresholds, such as N = 4 or 5, yields a more Pacific "ENSO-like" feature (not shown), but the added high frequencies by this wider filter are not normally included in the definition of the IPO. Figure 8b, d shows the spatial pattern and PC of the third EOF of the low-pass filtered SST. It has two centers of action, one located in the North Pacific and one in the North Atlantic, with the stronger Pacific center resembling that from the PDO.

In Fig. 9a, we decompose the IPO index, defined as the second PC of the 13-year low-pass filtered SST, into its components. Only the first four components are shown as these add up to the IPO index closely. The ENSO component is almost zero, as the interannual frequencies of this component are mostly removed by the low-pass filter. The passed frequencies in Fig. 9a are dominated by that of the AMO in the multidecadal range. So the IPO, if defined as the second PC, is actually mostly the AMO, when the decadal low-pass filtered is used in its definition. Figure 9b shows the results if the IPO is defined as the third PC of the 13-year low-passed filtered SST. Its components consist of a different proportions of ENSO, PDO and AMO, with a larger PDO component and smaller AMO component compared to the second PC. The ENSO component is again much reduced by

Fig. 7 The global-mean surface land-plus-ocean temperature. Similar to Fig. 5, but for the land-plus-ocean surface temperature
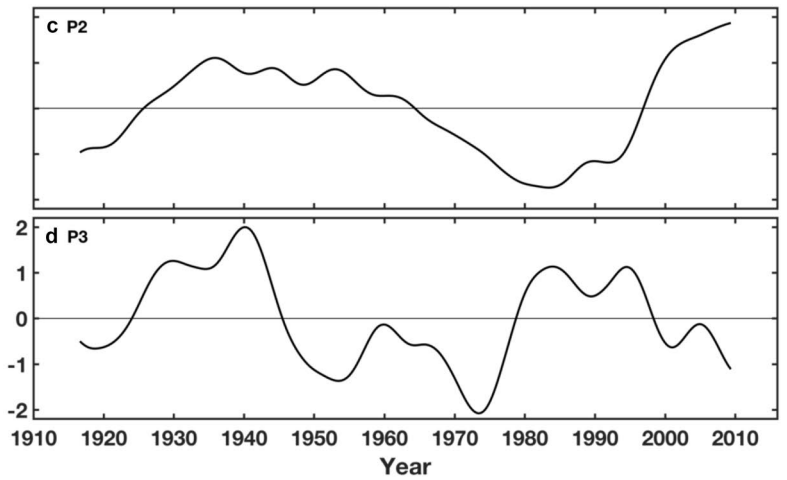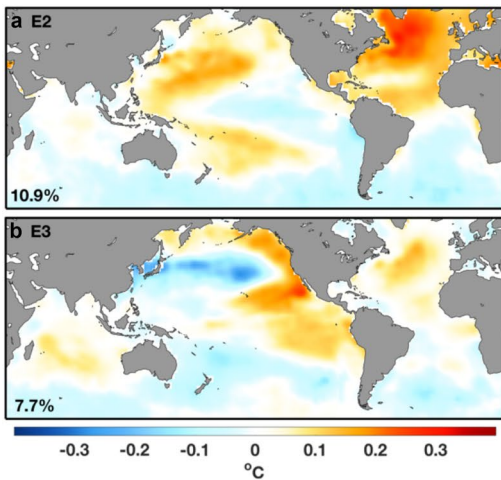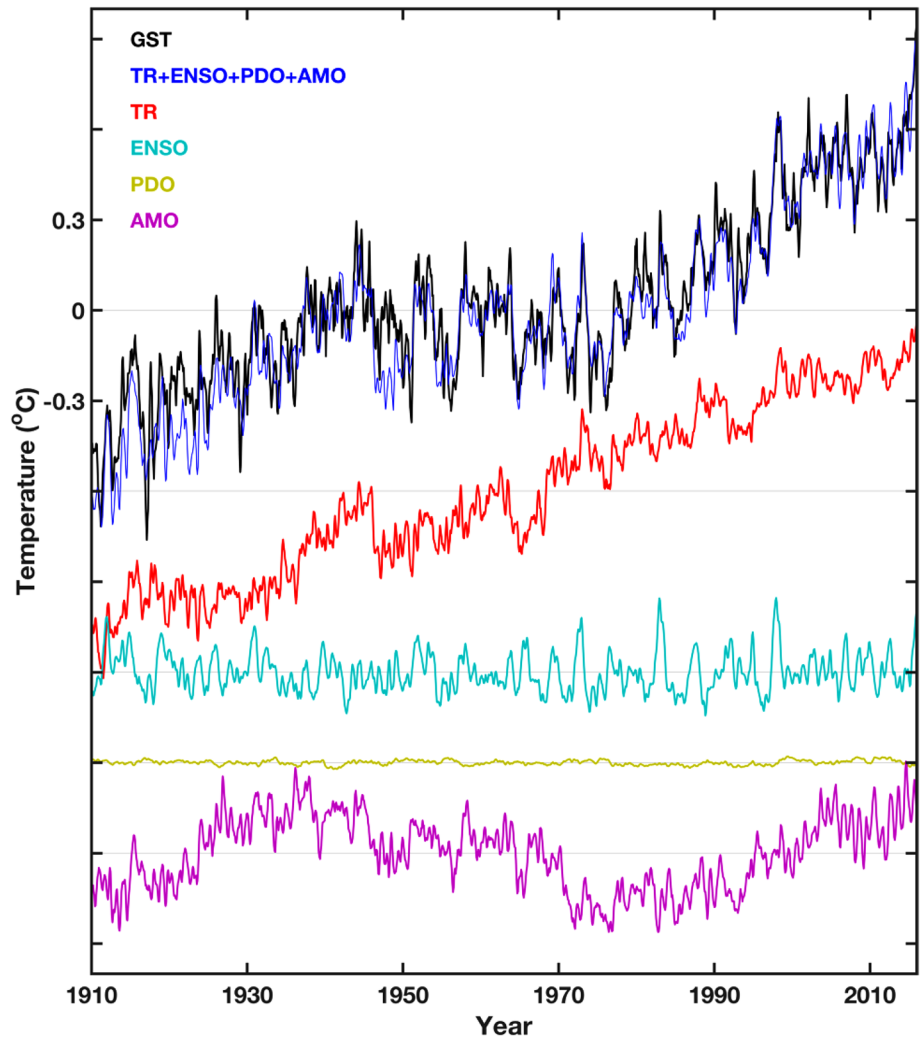
Fig. 8 EOF2 and PC2 of the 13-year filtered SST (top panels). EOF3 and PC3 (bottom panels)
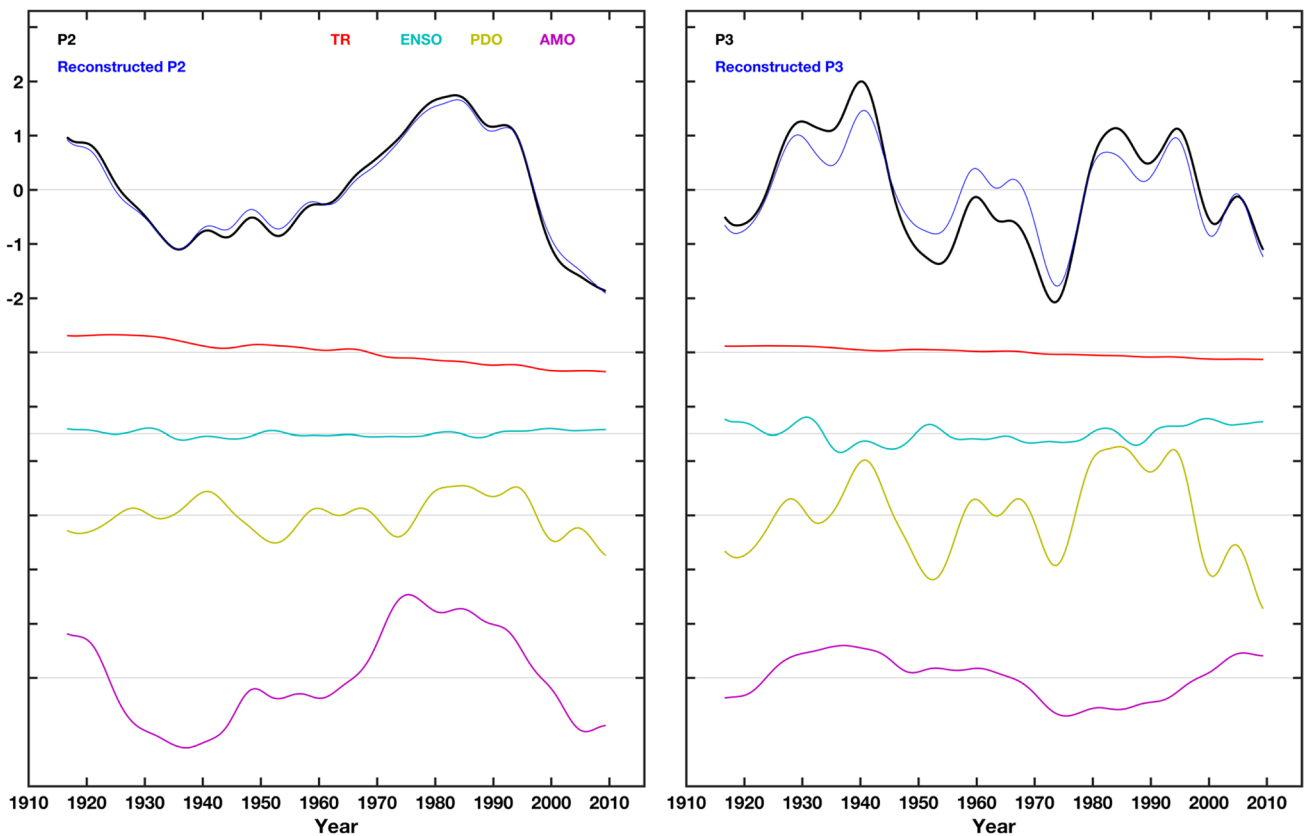
Fig. 9 Decomposition of the second EOF of 13-year low-pass filtered SST into its components, as a function of time (left panel), and similarly for the third EOF of the low-pass filtered SST(right panel)

decadal low-pass filtering, while the global mean of the PDO is almost zero. So the global mean of this IPO (third EOF/PC of decadally filtered SST) is almost zero (magnitudes will be given later).

The global mean of E_2 is 0.018 K, while that of E_3 is 0.0032 K, a factor of 6 smaller. This result is consistent with the different proportions of AMO vs PDO in the two modes. The surprising finding here is that contributions by E_2 and E_3 to the GSST are both so small. It turns out, since the IPO is defined using a conventional EOF analysis, the variations in the global mean is actually mostly in the first EOF/PC, similar to the situation of the conventional EOF decomposition of unfiltered data mentioned previously in Sect. 3. The conclusion is that, whether it is defined as the second or third PC of the low-pass filtered SST, the contribution of the IPO to the GSST is negligible.
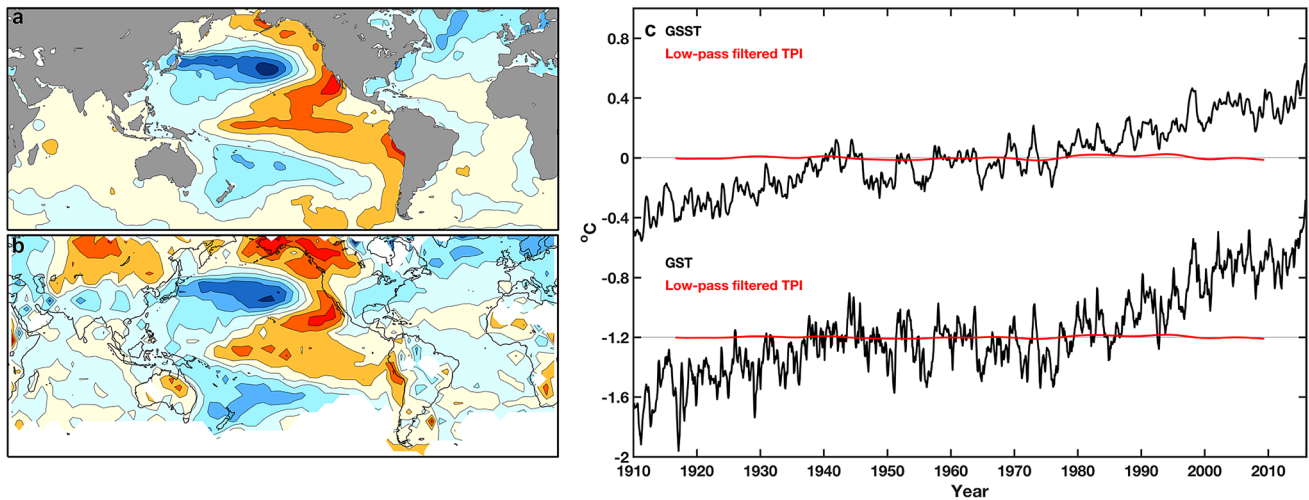
6 The TPI

As an alternative to using EOF analysis of the low-passed SST to define the IPO, Henley et al. (2015) proposed using

the difference of SSTs in three regions in the Pacific to define an IPO Tripole Index (TPI):

$$TPI = T_2 - 0.5(T_1 + T_3).$$

The three regions are: T_2 the central and eastern equatorial Pacific (10°S–10°N, 170°E–90°W), T_1 the Northwest Pacific (25°N–45°N, 140°E–145°W), and T_3 the Southwest Pacific (50°S–15°S, 150°E–160°W). The index is filtered using a 13-year low-pass filter to mimic the IPO index. The regressed spatial pattern of the low-passed TPI is shown in Fig. 10a, which is similar to that in Henley et al. (2017), and is close to, but not the same as the "ENSO-like" EOF in Fig. 2. The pattern is Pacific dominated, but compensating. The unfiltered TPI index (Henley et al. 2017) consists mainly of ENSO and the PDO (not shown). The low-pass filtering greatly reduces the ENSO component, leaving mostly the PDO, which has an almost zero global mean. The global mean of TPI is shown in Fig. 10c in red, while the GSST is shown in black. The TPI explains very little, about 0.05 °C, of the GSST variations about the trend. Figure 10d shows the global mean of the global surface temperature regressed onto the TPI index. It contributes even less to the GST (than to GSST), for the reason already discussed in Sect. 4.

Fig. 10 The Tripole Index and its global mean SST. **a** The global SST regressed onto the 13-year low pass filtered TPI index. **b** The global surface temperature regressed onto the 13-year low pass filtered TPI index. The contribution of the TPI to GSST is obtained by multiplying the global mean of the regressed SST spatial pattern by the TPI time series in (**c**). In (**d**) the global mean contribution of TPI to GST is obtained by multiplying the global mean of the regressed surface (land + ocean) temperature by the TPI time series

7 Conclusion and discussion

In the presence of monotonically increasing atmospheric concentration of greenhouse gases, the part of surface temperature that is the forced response should be generally increasing. The observed variation about this secular trend can be explained by the contribution of internal (unforced) variability or by time-varying aerosol forcing. Models have the ability to separate the forced from the unforced variability, with the former given by the ensemble mean. Some authors adopted a hybrid model-observational analysis by subtracting from the observed GST the modeled ensemble mean (Dai et al. 2015; Kosaka and Xie 2016; Smith et al. 2016; Dong and McPhaden 2017). This approach requires an assumption that the models can simulate the observed internal variability correctly. Since the present work is empirical, it does not definitively distinguish between the forced and unforced response. Another caveat is that our method includes only the contribution of the global-mean surface temperature by the direct (SST) and secondary (via teleconnection) of the effect of SST-based climate modes but does not include the possible other more complicated intermediate steps. Nevertheless it is hoped that the space–time information provided by our study can shed more light on the climate modes in different time scale ranges and on their role in affecting the global mean surface temperature.

It has been proposed that ENSO, PDO, IPO and AMO can contribute to the variations in the global mean surface temperature. Our result is shown in Figs. 5 and 7:

1. In addition to an increasing global warming mode (a positive trend since 1910), the multidecadal AMO mode with its center of action in the Atlantic contributes the most to the variation in the global mean SST and global mean land-plus-ocean surface temperature. Its variation from trough to peak is comparable to the centennial linear trend of GST.

2. ENSO's contribution is in the interannual time scale of 2–7 years.

3. PDO's contribution to the global mean surface temperature is small, about 1/10 that of the AMO.

4. The IPO is not an independent mode, but is a combination of AMO and PDO mixed together by the low-pass filter. Its contribution to the global-mean SST is given mostly by its AMO component. In any case the IPO, as defined by conventional EOF analysis, contributes very little to the global mean, whether it is taken as the second or third EOF of the low-pass filtered data. This is a problem of its definition using conventional EOF decomposition, not physics.

5. A better definition of a Pacific interdecadal variability is the IPO TPI index. This index involves only mean Pacific SST in three regions. Its main components are ENSO and PDO. When decadally filtered, the ENSO contribution is removed and so the TPI measures mostly the PDO. Its global mean is nearly zero.

How do the above listed results reconcile with the prevailing view that it is the IPO that causes the slowdown in global mean surface temperature during 1998–2012, called the "hiatus"? Some of the evidence of the role of IPO was based on the time series of the global mean surface temperature variation and that of the IPO being in phase. As we have shown here, the contribution of the IPO to the global mean

is mostly by the AMO component contained in the IPO (see Fig. 9 and conclusion #4 above). In this regard, the IPO is "Pacific" in name only. There has been in recent decades a tendency of Pacific trade winds intensifying and the SST tending to a La Nina state of cold eastern equatorial Pacific (England et al. 2014). However, as the trade winds blow the warm SST westward, there is compensating warm SST in the western Pacific. When the SST is averaged over the Pacific there is no net cooling trend in the tropical Pacific. Drijfhout et al. (2014) in a model setup specified both surface air temperature (SAT) and SST in the eastern Tropical Pacific from observation, and found "colder eastern tropical Pacific SSTs stand out, but the increase in heat uptake in the area is less prominent, confirmed by heat flux estimates". Larger heat uptake increase was found instead in the Atlantic and the Southern Ocean. When a cold SST from observation was specified in the eastern equatorial Pacific by other authors in a model that has a too-warm SAT, an anomalous heat uptake occurs in the eastern Pacific in the model, where there is an artificial large difference between the model SAT and the prescribed SST, giving the impression that this region of the Pacific is the sink responsible for the global SAT slowdown.

References

Barnett TP (1984) Long-term trends in surface-temperature over the oceans. Mon Weather Rev 112(2):303–312

Booth B. B. B., Dunstone NJ, Halloran PR, Andrews T, Bellouin N (2012) Aerosols implicated as a prime dirver of twentieth-century North Atlantic climate variability. Nature 484(7393):228–232

Brohan P, Kennedy JJ, Harris I, Trett S. F. B., Jones PD (2006). Uncertainty estimates in regional and global observed temperature changes: a new data set from 1850. J Geophys Res 111(D12106). doi:10.1029/2005JD006548

Chen X, Wallace JM (2016) Orthogonal PDO and ENSO indices. J Clim 29:3883–3892

Chen X, Wallace JM, Tung KK (2017) Pairwise-rotated EOF of global SST. J Clim 30:5473–5489. doi:10.1175/JCLI-D-16-0786.1

Dai A, Fyfe JC, Xie S-P, Dai X (2015) Decadal modulation of global surface temperature by internal climate variability. Nat Clim Change 5:555–559

Delworth TL, Mann ME (2000) Observed and simulated multidecadal variability in the Northern Hemisphere. Clim Dyn 16:661–676

Deser C, Wallace JM (1987) El-Niño events and their relation to the Southern Oscillation—1925–1986. J Geophys Res 92(C13):14189–14196

Deser C, Wallace JM (1990) Large-scale atmospheric circulation features of warm and cold episodes in the tropical Pacific. J Clim 3(11):1254–1281

Dong L, McPhaden MJ (2017) The role of external forcing and internal variability in regulating global mean surface temperatures on decadal timescales. Environ Res Lett 12:034011

Drijfhout SS, Blaker AT, Josey SA, Nurser A. J. G., Sinha B, Balmaseda MA (2014) Surface warming hiatus caused by increased heat uptake across multiple ocean basins. Geophys Res Lett 41

Enfield DB, Mestas-Nunez AM, Trimble PJ (2001) The Atlantic multidecadal oscillation and its relation to rainfall and river flows in the continental U.S. Geophys Res Lett 28:2077–2080

England MH, McGregor S, Spence P, Meehl GA, Timmermann A, Cai W, Gupta AS, McPhaden MJ, Purich A, Santoso A (2014) Recent intensification of wind-driven circulation in the Pacific and the ongoing warming hiatus. Nat Clim Change 4:222–227

Folland CK, Parker DE (1995) Correction of instrumental biases in historical sea-surface temperature data. Q J Roy Meteor Soc 121(522):319–367

Folland CK, Palmer TN, Parker DE (1986) Sahel rainfall worldwide sea temperatures. Nature 320(6063):602–606

Folland CK, Parker D, Colman AW (1999) Large scale modes of ocean surface temperature since the late nineteenth century. Beyond El Nino: Decadal and Interdecadal Climate Variability. A. Navarra

Henley BJ, Gergis J, Karoly DJ, Power S, Kennedy JJ, Folland CK (2015) A Tripole Index for the interdecadal Pacific oscillation. Clim Dyn 45:3077–3090

Henley BJ, Meehl GA, Power S, Folland CK, King AD, Brown JN, Karoly DJ, Delage F, Gallant A. J. E., Freund M, Neukom R (2017). Spatial and temporal agreement in climate model simulations of the Interdecadal pacific oscillation. Environ Res Lett 12(044011)

Horel JD, Wallace JM (1981) Planetary-scale atmospheric phenomena associated with the Southern oscillation. Mon Weather Rev 109:813–829

Hosking JS, Karoly D (1981) The steady linear response of a spherical atmosphere to thermal and orographic forcing. J Atmos Sci 38:1179–1196

Huang NE, Shen Z, Long SR, Wu M. L. C., Shih HH, Zheng QN, Yen NC, Tung CC, Liu HH (1998). The empirical mode decomposition and the Hilbert spectrum for nonlinear and non-stationary time series analysis. Proc R Soc Lond Ser a Math Phys Eng Sci 454(1971): 903–995

Knight JR, Allan RJ, Folland CK, Vellinga M (2005) A signature of persistent natural thermohaline circulation cycles in observed climate. Geophys Research Lett. 32(L20708). doi:10.1029/2005GL024233

Kosaka Y, Xie S-P (2016) The tropical Pacific as a key pacemaker of the variable rates of global warming. Nature Geosci 9:669–673

Mantua NJ, Hare SR, Zhang Y, Wallace JM, Francis RC (1997) A pacific interdecadal climate oscillation with impacts on salmon production. B Am Meteorol Soc 78(6):1069–1079

McPhaden MJ, Zebiac SE, Glantz MH (2006) ENSO as an integrating concept in earth science. Science 314:1740–1745

Meehl GA, Hu A, Santer B, Xie S-P (2016) Contribution of the Interdecadal Pacific oscillation to twentieth-century global surface temperature trends. Nat Clim Change 6:1005–1008

Minobe S (1999) Resonance in bidecadal and pentadecadal climate oscillations over the North Pacific: role in climatic regime shifts. Geophys Res Lett 26(7):855–858

Morice CP, Kennedy JJ, Rayner NA, Jones PD (2012) Quantifying uncertainties in global and regional temperature change using

an ensemble of observational estimates: the HadCRUT4 data set. J Geophys Res. 117. doi:10.1029/2011JD017187

Newman M, Compo GP, Alexander MA (2003) ENSO-forced variability of the Pacific decadal oscillation. J Clim 16:3853–3857

Newman M, et al (2016) The Pacific decadal oscillation, revisited. J Clim 29:4399–4427

Parker D, Folland CK, Scaife AA, Knight J, Colman AW, Baines P, Dong B (2007) Decadal and multidecadal variability in the climate change background. J Geophys Res 112:D18115

Power S, Casey T, Folland C, Colman A, Mehta V (1999) Inter-decadal modulation of the impact of ENSO on Australia. Clim Dynam 15(5):319–324

Sarachik E, Cane MA (2010). The El Nino-Southern oscillation phenomenon. Cambridge University Press, Cambridge

Schlesinger ME, Ramankutty N (1994) An oscillation in the global climate system of period 65–70 years. Nature 367:723–726

Schlesinger BM, Ramankutty N, Andronova N (2000) Temperature oscillations in the North Atlantic. Science 28:547–548

Simmons A, Wallace JM, Branstator G (1983) Barotropic wave propagation and instability and atmospheric teleconnection patterns. J Atmos Sci 40:1363–1392

Smith TM, Reynolds RW, Peterson TC, Lawrimore J (2008) Improvements to NOAA's historical merged land-ocean surface temperature analysis (1880–2006). J Clim 21:2283–2296

Smith DM, Booth B. B. B., Dunstone NJ, Eade R, Hermanson L, Jones GS, Scaife AA, Sheen KL, Thompson V (2016) Role of volcanic and anthropogenic aerosols in the recent global surface warming slowdown. Nat Clim Change 6(10):936–940

Thompson DWJ, Wallace JM, Jones PD, Kennedy JJ (2009) Identifying signatures of natural climate variability in time series of global-mean surface temperature: methodology and insights. J Climate 22:6120–6141

Trenberth KE (2015) Has there been a hiatus? Science 349:691–692

Wallace JM, Gutzler D (1981) Teleconnections in the geopotential height field during the Northern Hemisphere winter. Mon Weather Rev 109:784–812

Wu Z, Huang NE (2009) Ensemble empirical mode decomposition: a noise-assisted data analysis method. Adv Adapt Data Anal 1:1–14

Wu Z, Huang NE, Long SR, Peng CK (2007) On the trend, detrending and variability of nonlinear and non-stationary time series. Proc Natl Acad Sci USA 104:14889–14894

Wu Z, Huang NE, Wallace JM, Smoliak B, Chen X (2011) On the time-varying trend in global-mean surface temperature. Clim Dyn 37:759–773

Zhang Y, Wallace JM, Battisti DS (1997) ENSO-like interdecadal variability: 1900–93. J Clim 10:1004–1020

Zhang R, Delworth T, Sutton R, Hodson D. L. R., Dixon KW, Held I. M. H., Marshall Y., J., Ming Y, Msadeck R, Robson J, Rosati AJ, Ting M, Vecchi GA (2013) Have aerosols caused the observed Atlantic multidecadal variability? J Atmos Sci 70:1135–1144

Zhou J, Tung KK (2013) Deducing the multi-decadal anthropogenic global warming trend using multiple regression analysis. J Atmos Sci 70(1):3–8